Mendeleev Communications

Mendeleev Commun., 2025, **35**, 569–572

Partial lead substitution as a tool to manage the light-induced recrystallization and photostability of mixed-cation lead halide perovskites

Marina I. Ustinova,[a,b] Gennady V. Shilov,[a] Denis V. Korchagin,[a] Nadezhda N. Dremova,[a] Pavel A. Troshin,*[c,a] Sergey M. Aldoshin[a] and Lyubov A. Frolova*[a]

[a] *Federal Research Center of Problems of Chemical Physics and Medicinal Chemistry, Russian Academy of Sciences, 142432 Chernogolovka, Moscow Region, Russian Federation. E-mail: lyuanfro@gmail.com*
[b] *Centre for Hybrid and Organic Solar Energy, Department of Electronic Engineering, University of Rome Tor Vergata, 00133 Rome, Italy*
[c] *Zhengzhou Research Institute, Harbin Institute of Technology, 450003 Zhengzhou, China*

DOI: 10.71267/mencom.7697

Substitution of Pb^{2+} ions in lead halide perovskite $Cs_{0.12}FA_{0.88}PbI_3$ (FA is formamidinium cation) was investigated to address the issues of its phase stability and photostability. The incorporation of optimally selected Nd^{3+}, Tb^{3+} and Er^{3+} cations into $Cs_{0.12}FA_{0.88}Pb_{0.99}M_{0.02/n}I_3$ films significantly suppressed the light-induced recrystallization and photodegradation, maintaining the morphology, optical properties and phase composition after 9000 h of light exposure, and improved the efficiency and operational stability of perovskite solar cells.

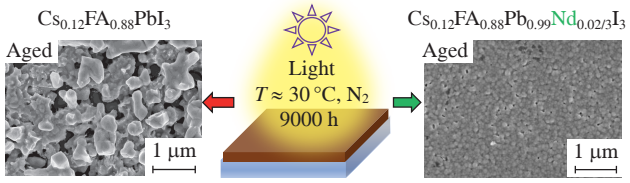

Keywords: perovskite solar cells, $Cs_{0.12}FA_{0.88}Pb_{0.99}I_3$, phase stability, photostability, light-induced recrystallization, partial lead substitution, long-term stability, operational stability.

Lead halide perovskites have been a groundbreaking discovery in materials science and electronics, enabling perovskite solar cells (PSCs) to achieve significant improvements in power conversion efficiency (PCE) from 3.9% in 2009 to over 26.5% in 2024.[1–3] Unlike silicon solar cells, PSCs exhibit defect tolerance, allowing them to be fabricated from standard chemically pure materials without extensive purification.[4] In addition, their production *via* cost-effective, high-throughput printing and coating technologies makes them highly attractive.[5–8] However, their commercial viability is hampered by poor operational stability.[9–11] Recent studies have highlighted the instability of methylammonium (MA)-based lead halides, prompting a shift to perovskites based on formamidinium (FA) and cesium (Cs) cations.[12–14] These 'multication perovskites' allow tuning of properties by changing the cation ratio,[15–18] but problems of phase segregation under light or radiation exposure remain.[19,20] To improve the stability of perovskite materials, composition engineering using organic additives[21,22] or metal salts[23,24] has been used. We recently demonstrated that B-site modification by replacing 1 mol% of Pb^{2+} ions with other metal ions significantly enhances the photostability of $CsPbI_3$ and $MAPbI_3$ films.[21,22,25,26] Here, we extend this approach to the 'double-cation' formulation $Cs_{0.12}FA_{0.88}PbI_3$ to improve both the photostability and photovoltaic performance of PSCs.

To evaluate the effect of different modifying cations on the properties of $Cs_{0.12}FA_{0.88}PbI_3$ absorber films, a very simple experimental approach was used, which basically repeated the strategy we developed for $CsPbI_3$ and $MAPbI_3$ perovskites.[25,26] Individual solutions of $Cs_{0.12}FA_{0.88}PbI_3$ (1.35 M) and $Cs_{0.12}FA_{0.88}MI_{n+1}$ (0.2–1.35 M, depending on the solubility of the halide MI_n) in a 1 : 10 (v/v) dimethyl sulfoxide–*N*,*N*-dimethylacetamide (DMAc) solvent mixture were mixed together in appropriate ratios to achieve the $Cs_{0.12}FA_{0.88}Pb_{0.99}M_{0.02/n}I_3$ precursor stoichiometry immediately before film deposition by spin-coating (Figure S1, see Online Supplementary Materials).[†] It is important to avoid long-term storage of individual $Cs_{0.12}FA_{0.88}MI_{n+1}$ precursor solutions and, in particular, mixed $Cs_{0.12}FA_{0.88}Pb_{0.99}M_{0.02/n}I_3$ precursor solutions, since some metal iodides MI_n tend to form crystal solvate complexes with solvent molecules, which precipitate and change the solution stoichiometry. Thus, we isolated and characterized by X-ray diffraction[‡] single crystals of $Eu(DMAc)_6I_2$ **1** and $Sr(DMAc)_6I_2$ **2** (Figures S2–S4, see Online Supplementary Materials), which were precipitated from the corresponding solutions.

The degradation of the perovskite films was monitored by periodically measuring their UV-VIS absorption spectra and plotting their evolution with increasing aging time [Figure 1(*a*)]. Thus, the reference non-modified $Cs_{0.12}FA_{0.88}PbI_3$ films demonstrated dramatic

[†] Thin films of perovskite formulations $Cs_{0.12}FA_{0.88}Pb_{0.99}M_{0.02/n}I_3$ were prepared by spin-coating the precursor solution (50 μl) on glass substrates at 3600 rpm followed by dropping toluene to induce film crystallization. The deposited films were annealed at 120 °C for 5 min and subjected to aging tests under continuous exposure to white light of 90 ± 5 mW cm^{-2} as described previously.[25,26] Given the good overlap of the emission spectrum of the LED light source used and the absorption spectrum of the perovskite film, the samples received under our test conditions the photon dose provided by standard solar AM1.5G irradiation of 150 mW cm^{-2}. All experiments, including film preparation, aging tests and measurements such as UV-VIS absorption spectra, were conducted under strictly controlled anoxic conditions (with O_2 and H_2O levels below 0.1 ppm) inside glove boxes. This ensured that the observed sample behavior was intrinsic and not affected by the presence of ambient moisture or oxygen.

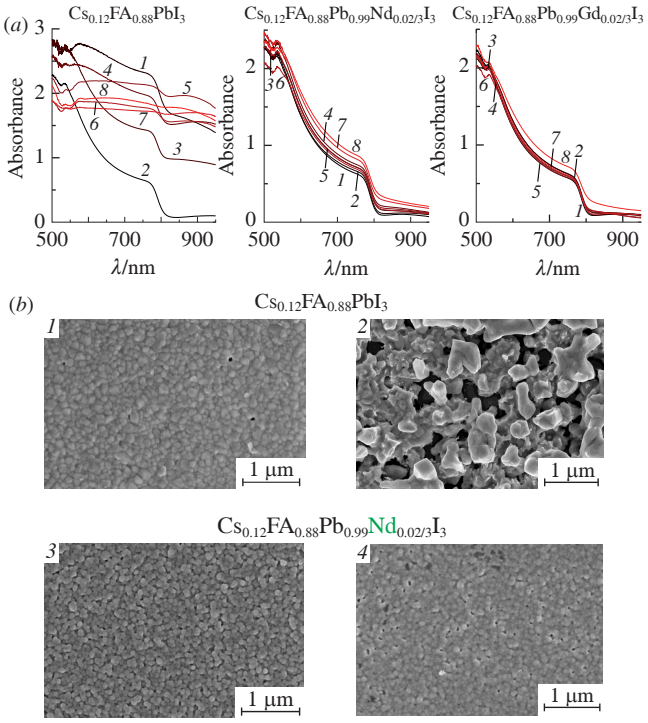

Figure 1 (*a*) Evolution of the UV-VIS spectra of the non-modified $Cs_{0.12}FA_{0.88}PbI_3$ film (reference) and modified $Cs_{0.12}FA_{0.88}Pb_{0.99}M_{0.02/3}I_3$ (M = Nd, Gd) films measured after (*1*) 0, (*2*) 500, (*3*) 900, (*4*) 1500, (*5*) 3200, (*6*) 5000, (*7*) 7500 and (*8*) 9000 h of light soaking. (*b*) SEM images of (*1*),(*2*) reference and (*3*),(*4*) Nd^{3+}-loaded perovskite films (*1*),(*3*) before and (*2*),(*4*) after 9000 h of light soaking.

spectral changes even after short-term exposure to light, and after 500 h of illumination the absorption profile became almost featureless due to strong light scattering. This kind of spectral behavior is related to the light-induced recrystallization of complex lead halides.[19,30] In contrast, the complex $Cs_{0.12}FA_{0.88}Pb_{0.99}M_{0.02/n}I_3$ materials loaded with different M^{n+} cations exhibited much higher resistance to light-induced recrystallization. Thus, the optical spectra of the $Cs_{0.12}FA_{0.88}Pb_{0.99}Nd_{0.02/3}I_3$ and $Cs_{0.12}FA_{0.88}Pb_{0.99}Gd_{0.02/3}I_3$ films were remarkably stable during 9000 h of light exposure, and minor light scattering appeared only at the end of the experiment [see Figure 1(*a*)]. Scanning electron microscopy (SEM) images revealed a complete loss of the initial ordered granular morphology of the reference $Cs_{0.12}FA_{0.88}PbI_3$ films after 9000 h of light soaking, resulting in the formation of large micrometer-sized aggregates that are most likely responsible for the observed strong light scattering effect [Figure 1(*b*)]. According to SEM images, optimally modified films such as $Cs_{0.12}FA_{0.88}Pb_{0.99}Nd_{0.02/3}I_3$, on the contrary, completely retained the uniformity and ordered structure. Thus, the modification of $Cs_{0.12}FA_{0.88}PbI_3$ by replacing 1% of lead with optimally selected metal ions can effectively prevent light-induced recrystallization of the absorber, ensuring long-term operational stability of PSCs.

Next, the photochemical stability of $Cs_{0.12}FA_{0.88}Pb_{0.99}M_{0.02/n}I_3$ films modified with different metal cations was evaluated. X-ray diffraction (XRD) patterns of representative films before and after 9000 h of light soaking are shown in Figure S5. The reference non-modified $Cs_{0.12}FA_{0.88}PbI_3$ films degraded very strongly, forming a predominant PbI_2 phase and a considerable amount of metallic lead Pb^0 [Figure S5(*a*)]. The photochemical aging becomes even more severe when suboptimal modifying cations are selected, as shown for $Cs_{0.12}FA_{0.88}Pb_{0.99}Mg_{0.01}I_3$, which degraded almost completely to PbI_2 and Pb^0, thus leaving virtually no surviving perovskite phase [Figure S5(*b*)]. On the contrary, favorably modified materials showed impressively improved photostability. For example, $Cs_{0.12}FA_{0.88}Pb_{0.99}Nd_{0.02/3}I_3$ revealed the formation of just a minor amount of PbI_2 impurity phase after 9000 h of aging, while the major perovskite phase remained virtually intact [Figure S5(*c*)]. The XRD patterns for a broader range of systems are shown in Figure S6. It can be seen that the introduction of substitutional metal ions has a very strong effect on the photostability of the perovskite films and the composition of the resulting products.

Analysis of the XRD patterns of all the studied materials allowed us to determine the phase composition of the samples after 9000 h of light soaking [Figure S7(*a*)]. Some of the $Cs_{0.12}FA_{0.88}Pb_{0.99}M_{0.02/n}I_3$ materials demonstrated impressively enhanced photochemical stability due to the incorporation of metal cations such as Nd^{3+}, Tb^{3+}, Gd^{3+}, Er^{3+}, Lu^{3+} and to some extent La^{3+}. Interestingly, all of the most stable materials contained rare earth metal cations. Among the non-lanthanide cations, the strongest stabilization was caused by Sn^{4+} ions, and much weaker effects were exerted by Sn^{2+}, Ni^{2+}, Zn^{2+}, Sr^{2+} and Pt^{2+} ions. Many systems, for example, incorporating cations such as Bi^{3+}, Y^{3+}, Dy^{2+}, Yb^{2+}, Eu^{2+}, Co^{2+}, Cd^{2+}, Cu^{+}, Mg^{2+}, Ba^{2+}, Ca^{2+} and Ge^{2+}, demonstrated accelerated aging compared to the reference non-modified $Cs_{0.12}FA_{0.88}PbI_3$ films. The obtained results do not point to any clear correlation between the nature of the metal cations (*i.e.*, their valence state and position in the periodic table) and their effect on the photostability of lead halide perovskite films. It only seems that divalent rare earth metal cations such as Yb^{2+} and Eu^{2+} have a negative impact on the photostability of $Cs_{0.12}FA_{0.88}Pb_{0.99}M_{0.02/n}I_3$ films, while trivalent lanthanide cations mostly cause a strong stabilization effect. The enhanced stability of perovskite materials achieved by cationic substitution of lead at the B-site of perovskite structure may be due to several key factors, including reducing lattice strain, minimizing structural distortions and suppressing ion migration.

Another figure of merit for analyzing the photostability of differently modified $Cs_{0.12}FA_{0.88}Pb_{0.99}M_{0.02/n}I_3$ films was based on optical spectroscopy data. We could not use the normalized film absorption as a descriptor of material stability directly, since it varied greatly for the least stable materials due to strong light scattering effects. Therefore, to reconstruct the aging dynamics of the perovskite films and mitigate the contribution of light scattering, we proposed to use the parameter A^*, which is calculated as follows:

$$A^* = [A_t^{570\ nm} - A_t^{980\ nm}]/[A_0^{570\ nm} - A_0^{980\ nm}],$$

where A_t is the film absorption after aging time t and A_0 is the initial absorption of the film. We chose two characteristic wavelengths: 570 nm, corresponding to the maximum of the perovskite absorption band, and 980 nm, the energy of which is below the optical band gap of perovskite and, therefore, its intensity is affected only by light scattering. Even though this approach provides just a rough approximation, it turned out to be very useful for comparing

‡ *Crystal data for* **1**. $C_{24}H_{54}EuI_2N_6O_6$, M = 928.49, trigonal, space group $P\bar{3}$, $a = b$ = 12.0935(6) and c = 7.1307(4) Å, V = 903.2(1) Å^3, Z = 1, d_{calc} = 1.707 g cm^{-3}, μ = 3.486 mm^{-1}, $F(000)$ = 457, the final R_1 = 0.0368, wR^2 = 0.0873 and GOOF = 1.079 for 2861 observed reflections with $I > 2\sigma(I)$.

Crystal data for **2**. $C_{24}H_{54}SrI_2N_6O_6$, M = 864.15, trigonal, space group $P\bar{3}$, $a = b$ = 12.0602(4) and c = 7.1300(2) Å, V = 898.10(6) Å^3, Z = 1, d_{calc} = 1.598 g cm^{-3}, μ = 3.260 mm^{-1}, $F(000)$ = 432, the final R_1 = 0.0376, wR^2 = 0.0797 and GOOF = 0.927 for 2994 observed reflections with $I > 2\sigma(I)$.

Single crystal X-ray diffraction measurements were carried out at 100(2) K on an Agilent XCalibur CCD diffractometer with an EOS detector with graphite-monochromated MoKα radiation (λ = 0.71073 Å). Data collection, determination and refinement of unit cell parameters were carried out using the CrysAlis PRO software package.[27] The structures were solved by direct methods, and non-hydrogen atoms were located from a trial structure and then refined anisotropically with SHELXTL[28,29] using full-matrix least-squares procedures based on F^2 values. Hydrogen atom positions were fixed geometrically at calculated distances and refined using the riding model constraints.

CCDC 2406039 and 2406040 contain the supplementary crystallographic data for this paper. These data can be obtained free of charge from The Cambridge Crystallographic Data Centre *via* https://www.ccdc.cam.ac.uk.

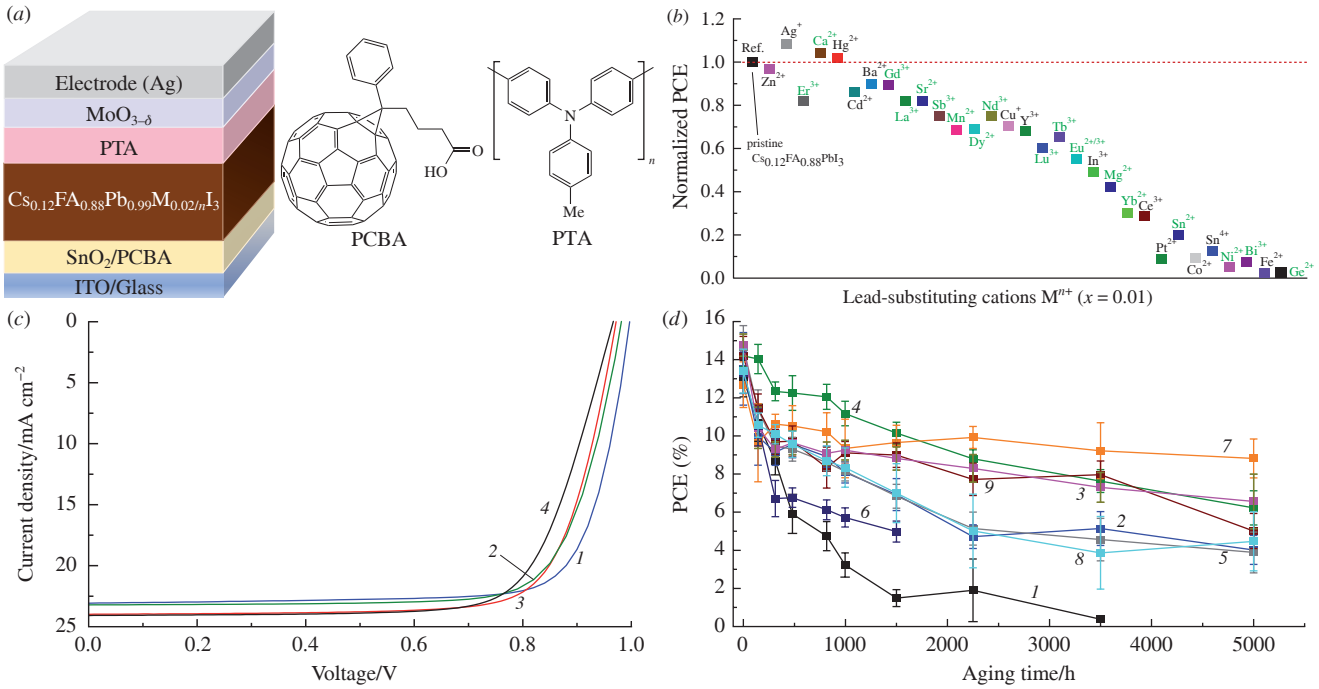

Figure 2 (*a*) Architecture of n-i-p PSCs and interlayer materials used. (*b*) Overview of the photovoltaic performance of $Cs_{0.12}FA_{0.88}Pb_{0.99}M_{0.02/n}I_3$ materials. The achieved PCE values were normalized to that of the reference $Cs_{0.12}FA_{0.88}PbI_3$-based cell. (*c*) Current–voltage characteristics of the best-performing cells, M^{n+} (*x*): (*1*) Er^{3+} (0.001), (*2*) Ag^+ (0.01), (*3*) Ba^{2+} (10^{-5}) and (*4*) reference. (*d*) Operational stability of PSCs with different absorber materials tested at 90 mW cm^{-2} LED light (equivalent to ~150 mW cm^{-2} AM1.5G illumination) under open-circuit conditions, M^{n+}(*x*): (*1*) reference, (*2*) Ca^{2+} (0.01), (*3*) Ba^{2+} (0.01), (*4*) Zn^{2+} (0.01), (*5*) Sr^{2+} (0.01), (*6*) $Eu^{2+/3+}$(0.01), (*7*) Zn^{2+} (0.03), (*8*) Sr^{2+} (0.03) and (*9*) Er^{3+} (0.01).

the aging dynamics of materials with complex compositions (Figure S8). The behavior of materials with different compositions is illustrated by diagrams of the A^* values obtained after 4000 and 9000 h of aging [Figure S7(*b*),(*c*)]. In general, a good correlation is observed between the optical characteristics of the films and their phase composition after 9000 h of light exposure: higher A^* values were obtained for systems with a higher fraction of the perovskite phase, which survived these aging conditions. Only for a few systems the high A^* value was inconsistent with the XRD data indicating severe degradation of the material. This is most clearly demonstrated by the example of $Cs_{0.12}FA_{0.88}Pb_{0.99}Fe_{0.01}I_3$ films, which showed an exceptionally high tendency for light-induced recrystallization leading to extreme light scattering, which was not compensated for by the A^* calculation algorithm. In this case, the A^* value for this system approaches 1.8 at the maximum and remains high until the end of the experiment mainly due to non-compensated light scattering (see Figure S8). Another system that showed a similar, but much less pronounced abnormal behavior is $Cs_{0.12}FA_{0.88}Pb_{0.99}Hg_{0.01}I_3$. Thus, optical spectroscopy has certain limitations for films that strongly scatter light, but in general it provides quite reliable assessment of the aging dynamics of lead halide perovskites.

Figure 2 shows the photovoltaic performance of compositionally different $Cs_{0.12}FA_{0.88}Pb_{0.99}M_{0.02/n}I_3$ absorber materials in PSCs assembled in the n-i-p configuration.

It was found that only a few substituent metal cations, namely Ag^+, Ca^{2+} and Hg^{2+}, were able to provide higher efficiencies in solar cells than the reference non-modified perovskite $Cs_{0.12}FA_{0.88}PbI_3$ [Figure 2(*b*)]. However, none of these cations actually improved the intrinsic photostability of the perovskite absorber films. The incorporation of Nd^{3+} and Tb^{3+} cations in the $Cs_{0.12}FA_{0.88}Pb_{0.99}M_{0.02/n}I_3$ absorber films significantly compromised their photovoltaic performance, while less significant deterioration of the solar cell characteristics was observed when using Gd^{3+} and Er^{3+} as substituents for lead. Therefore, we further optimized the PSCs based on a selected group of $Cs_{0.12}FA_{0.88}Pb_{0.99}M_{0.02/n}I_3$ absorber materials by systematically varying the M^{n+} cation loading over a wide concentration range. Thus, for materials with the general stoichiometric formula $Cs_{0.12}FA_{0.88}Pb_{1-x}M_{0.02x/n}I_3$, we varied the *x* value (M^{n+} cation loading) from 10^{-5} to 10^{-1}, as shown, for example, for Ca^{2+}, Sr^{2+} and Er^{3+} in Figure S9. Using this approach, we found optimal loadings for several cations that provided higher PCEs in PSCs than the reference non-modified double-cation perovskite $Cs_{0.12}FA_{0.88}PbI_3$ [Figure 2(*c*), Figure S10 and Table S1, see Online Supplementary Materials]. Thus, we demonstrated that partial lead substitution can be used not only as a tool to enhance the intrinsic photostability of absorber materials but also as an approach to improve the performance of PSCs.

The operational stability of PSCs is a very important issue that limits the commercial application of this highly promising photovoltaic technology. We investigated the stability of n-i-p PSCs fabricated using different $Cs_{0.12}FA_{0.88}Pb_{1-x}M_{0.02x/n}I_3$ absorber materials under continuous white light exposure (90 mW cm^{-2} LED light equivalent to ~150 mW cm^{-2} AM1.5G illumination). The cells were in the open-circuit state throughout the entire experiment, which is known to be the 'worst-case scenario' causing the most severe device degradation.[31] The reference solar cells based on non-modified $Cs_{0.12}FA_{0.88}PbI_3$ degraded almost completely after 1500 h of light soaking. On the contrary, PSCs based on modified absorber materials loaded with Er^{3+} and especially Zn^{2+} cations showed much higher operational stability [Fgure 2(*d*)]. Thus, the best cells based on $Cs_{0.12}FA_{0.88}Pb_{0.97}Zn_{0.03}I_3$ absorber films retained on average 67–70% of the initial performance after 5000 h of continuous aging under open-circuit conditions, which represents one of the best results achieved in this field so far.

It is noteworthy that the operational stability of the PSCs correlates quite well with the intrinsic stability of the corresponding absorber films. Thus, both thin films and devices with high Ba^{2+} and Eu^{2+} cation loadings showed quite fast degradation, while the systems loaded with Er^{3+} cations were generally much more stable. A notable exception was Zn^{2+}, which strongly enhanced the operational stability of the PSCs [see Figure 2(*d*)], while having a very modest positive effect on the intrinsic photostability of the corresponding absorber thin films (Figure S7). This apparent

contradiction is explained by the fact that Zn^{2+} is known to provide a very stable interface with MA-free lead halide perovskites.[32,33] Therefore, the positive effect of Zn^{2+} cations on the device level should be ascribed to the modification of the interface between SnO_2 and the perovskite absorber layer.

In summary, we have systematically investigated the effect of partial Pb^{2+} substitution on the intrinsic photostability and photovoltaic performance of the double-cation $Cs_{0.12}FA_{0.88}PbI_3$ perovskite films. It has been shown that many materials, especially those loaded with rare earth metal cations such as Nd^{3+}, Er^{3+}, Tb^{3+}, Lu^{3+} and La^{3+}, exhibited much higher stability under continuous light exposure compared to the reference non-modified films. The best absorber materials retained the original optical properties and single-phase composition after 9000 h of light exposure, which is one of the best results ever reported for perovskite absorber materials. Unfortunately, the most promising substituent ions, which greatly improved the photostability of perovskite absorber films, notably compromised their photovoltaic performance, so it was necessary to find a balance between these two effects. By optimizing the M^{n+} substituent cation loading in the active layer of PSCs, we achieved higher PCE values for a range of systems (containing Ca^{2+}, Sr^{2+}, Ba^{2+}, Ag^{+} and Er^{3+}) compared to the reference cells based on non-modified $Cs_{0.12}FA_{0.88}PbI_3$. Finally, we demonstrated a strong positive effect of Er^{3+} and Zn^{2+} substituent cations on the operational stability of PSCs, such that the best devices could retain 67–70% of the initial performance after 5000 h of continuous illumination under open-circuit conditions. These results demonstrate the enormous potential of Pb^{2+} substitution chemistry to enhance the photostability of absorber materials, improve device performance and extend their operational lifetime, thereby offering an additional avenue to the commonly used material science strategies for the development of efficient and stable PSCs.

This work was supported by the Ministry of Science and Higher Education of the Russian Federation [grant no. 075-15-2022-1217 (13.2251.21.0163)].

Online Supplementary Materials

Supplementary data associated with this article can be found in the online version at doi: 10.71267/mencom.7697.

References

1 A. Cuthbertson, *Hundreds of years after it was discovered, one material is about to change the world, The Independent,* 02 August 2023; https://www.independent.co.uk/tech/perovskite-solar-panels-renewable-energy-b2386049.html.

2 Editorial, *Nat. Mater.*, 2021, **20**, 1303; https://doi.org/10.1038/s41563-021-01127-8.

3 M. A. Green, E. D. Dunlop, M. Yoshita, N. Kopidakis, K. Bothe, G. Siefer, D. Hinken, M. Rauer, J. Hohl-Ebinger and X. Hao, *Prog. Photovoltaics*, 2024, **32**, 425; https://doi.org/10.1002/pip.3831.

4 Z. Guo, M. Yuan, G. Chen, F. Liu, R. Lu and W.-J. Yin, *Adv. Sci.*, 2024, **11**, 2305799; https://doi.org/10.1002/advs.202305799.

5 Y. Y. Kim, T.-Y. Yang, R. Suhonen, A. Kemppainen, K. Hwang, N. J. Jeon and J. Seo, *Nat. Commun.*, 2020, **11**, 5146; https://doi.org/10.1038/s41467-020-18940-5.

6 B. Parida, A. Singh, A. K. Kalathil Soopy, S. Sangaraju, M. Sundaray, S. Mishra, S. (F.) Liu and A. Najar, *Adv. Sci.*, 2022, **9**, 2200308; https://doi.org/10.1002/advs.202200308.

7 C. Chen, C. Ran, Q. Yao, J. Wang, C. Guo, L. Gu, H. Han, X. Wang, L. Chao, Y. Xia and Y. Chen, *Adv. Sci.*, 2023, **10**, 2303992; https://doi.org/10.1002/advs.202303992.

8 S. Valsalakumar, A. Roy, T. K. Mallick, J. Hinshelwood and S. Sundaram, *Energies*, 2023, **16**, 190; https://doi.org/10.3390/en16010190.

9 N. Ahn and M. Choi, *Adv. Sci.*, 2024, **11**, 2306110; https://doi.org/10.1002/advs.202306110.

10 T. A. Chowdhury, Md. Arafat Bin Zafar, Md. Sajjad-Ul Islam, M. Shahinuzzaman, M. A. Islam and M. U. Khandaker, *RSC Adv.*, 2023, **13**, 1787; https://doi.org/10.1039/D2RA05903G.

11 H. Zhu, S. Teale, M. N. Lintangpradipto, S. Mahesh, B. Chen, M. D. McGehee, E. H. Sargent and O. M. Bakr, *Nat. Rev. Mater.*, 2023, **8**, 569; https://doi.org/10.1038/s41578-023-00582-w.

12 S. Chen, X. Zhang, J. Zhao, Y. Zhang, G. Kong, Q. Li, N. Li, Y. Yu, N. Xu, J. Zhang, K. Liu, Q. Zhao, J. Cao, J. Feng, X. Li, J. Qi, D. Yu, J. Li and P. Gao, *Nat. Commun.*, 2018, **9**, 4807; https://doi.org/10.1038/s41467-018-07177-y.

13 T. T. Ava, A. Al Mamun, S. Marsillac and G. Namkoong, *Appl. Sci.*, 2019, **9**, 188; https://doi.org/10.3390/app9010188.

14 D. J. J. Tay, B. Febriansyah, T. Salim, M. Kovalev, A. Sharma, T. M. Koh, S. G. Mhaisalkar, J. W. Ager and N. Mathews, *Small*, 2025, **21**, 2403389; https://doi.org/10.1002/smll.202403389.

15 M. M. Byranvand, C. Otero-Martínez, J. Ye, W. Zuo, L. Manna, M. Saliba, R. L. Z. Hoye and L. Polavarapu, *Adv. Opt. Mater.*, 2022, **10**, 2200423; https://doi.org/10.1002/adom.202200423.

16 B. Ding, Y. Ding, J. Peng, J. Romano-deGea, L. E. K. Frederiksen, H. Kanda, O. A. Syzgantseva, M. A. Syzgantseva, J.-N. Audinot, J. Bour, S. Zhang, T. Wirtz, Z. Fei, P. Dörflinger, N. Shibayama, Y. Niu, S. Hu, S. Zhang, F. F. Tirani, Y. Liu, G.-J. Yang, K. Brooks, L. Hu, S. Kinge, V. Dyakonov, X. Zhang, S. Dai, P. J. Dyson and M. K. Nazeeruddin, *Nature*, 2024, **628**, 299; https://doi.org/10.1038/s41586-024-07228-z.

17 C. Zhao, Z. Zhou, M. Almalki, M. A. Hope, J. Zhao, T. Gallet, A. Krishna, A. Mishra, F. T. Eickemeyer, J. Xu, Y. Yang, S. M. Zakeeruddin, A. Redinger, T. J. Savenije, L. Emsley, J. Yao, H. Zhang and M. Grätzel, *Nat. Commun.*, 2024, **15**, 7139; https://doi.org/10.1038/s41467-024-51550-z.

18 F. Song, D. Zheng, J. Feng, J. Liu, T. Ye, Z. Li, K. Wang, S. (F.) Liu and D. Yang, *Adv. Mater.*, 2024, **36**, 2312041; https://doi.org/10.1002/adma.202312041.

19 A. G. Boldyreva, I. S. Zhidkov, S. Tsarev, A. F. Akbulatov, M. M. Tepliakova, Y. S. Fedotov, S. I. Bredikhin, E. Yu. Postnova, S. Yu. Luchkin, E. Z. Kurmaev, K. J. Stevenson and P. A. Troshin, *ACS Appl. Mater. Interfaces*, 2020, **12**, 19161; https://doi.org/10.1021/acsami.0c01027.

20 V. V. Ozerova, N. A. Emelianov, D. P. Kiryukhin, P. P. Kushch, G. V. Shilov, G. A. Kichigina, S. M. Aldoshin, L. A. Frolova and P. A. Troshin, *J. Phys. Chem. Lett.,* 2023, **14**, 743; https://doi.org/10.1021/acs.jpclett.2c03763.

21 C. Pereyra, H. Xie and M. Lira-Cantu, *J. Energy Chem.*, 2021, **60**, 599; https://doi.org/10.1016/j.jechem.2021.01.037.

22 N. N. Udalova, A. A. Petrov, E. M. Nemygina, K. R. Plukchi, E. A. Goodilin and A. B. Tarasov, *Mendeleev Commun.*, 2024, **34**, 840; https://doi.org/10.1016/j.mencom.2024.10.023.

23 R. Kour, S. Arya, S. Verma, J. Gupta, P. Bandhoria, V. Bharti, R. Datt and V. Gupta, *Global Challenges*, 2019, **3**, 1900050; https://doi.org/10.1002/gch2.201900050.

24 Q. Zhang, F. Hao, J. Li, Y. Zhou, Y. Wei and H. Lin, *Sci. Technol. Adv. Mater.*, 2018, **19**, 425; https://doi.org/10.1080/14686996.2018.1460176.

25 M. I. Ustinova, M. V. Lobanov, G. V. Shilov, N. N. Dremova, A. F. Akbulatov, L. G. Gutsev, I. S. Zhidkov, E. Z. Kurmaev, F. A. Prudnov, A. V. Ivanov, L. A. Frolova, S. M. Aldoshin and P. A. Troshin, *Adv. Funct. Mater.*, 2024, **35**, 2407571; https://doi.org/10.1002/adfm.202407571.

26 M. I. Ustinova, M. M. Mikheeva, G. V. Shilov, N. N. Dremova, L. Frolova, K. J. Stevenson, S. M. Aldoshin and P. A. Troshin, *ACS Appl. Mater. Interfaces*, 2021, **13**, 5184; https://doi.org/10.1021/acsami.0c18061.

27 *CrysAlis PRO* (version 171.35.19), Agilent Technologies UK Ltd., Yarnton, England, 2011.

28 G. M. Sheldrick, *Acta Crystallogr., Sect. A: Found. Crystallogr.*, 2008, **64**, 112; https://doi.org/10.1107/S0108767307043930.

29 G. M. Sheldrick, *Acta Crystallogr., Sect. C: Struct. Chem.*, 2015, **71**, 3; https://doi.org/10.1107/S2053229614024218.

30 A. F. Akbulatov, M. I. Ustinova, L. Gutsev, S. A. Tsarev, N. N. Dremova, I. Zhidkov, S. Yu. Luchkin, B. R. Ramachandran, L. Frolova, E. Z. Kurmaev, K. J. Stevenson, S. M. Aldoshin and P. A. Troshin, *Nano Energy*, 2021, **86**, 106082; https://doi.org/10.1016/j.nanoen.2021.106082.

31 K. Domanski, E. A. Alharbi, A. Hagfeldt, M. Grätzel and W. Tress, *Nat. Energy*, 2018, **3**, 61; https://doi.org/10.1038/s41560-017-0060-5.

32 M. M. Tepliakova, A. N. Mikheeva, L. A. Frolova, A. G. Boldyreva, A. Elakshar, A. V. Novikov, S. A. Tsarev, M. I. Ustinova, O. R. Yamilova, A. G. Nasibulin, S. M. Aldoshin, K. J. Stevenson and P. A. Troshin, *J. Phys. Chem. Lett.*, 2020, **11**, 5563; https://doi.org/10.1021/acs.jpclett.0c01600.

33 A. F. Akbulatov, I. S. Zhidkov, L. G. Gutsev, O. A. Krayevaya, N. A. Emelianov, G. V. Shilov, V. V. Ozerova, N. N. Dremova, E. Z. Kurmaev and P. A. Troshin, *Mater. Today Energy*, 2025, **47**, 101747; https://doi.org/10.1016/j.mtener.2024.101747.

Received: 2nd December 2024; Com. 24/7697